NORGES GEOTEKNISKE INSTITUTT

Prosjekt/rapportnr.: 20110112-00-1-TN Dato: 2012-05-18

Utarbeidet av: Dieter Issler / Tómas Jóhannsson

Prosjekt/rapporttitel: Analyse av sedimentkolonnemetoden ift. Karakterisering av sedimentenes avsetningsegenskaper. Dynamical Consistency Constraints on Entrainment and Deposition in Depth-Averaged Models of Snow Avalanches and Other Gravity Mass Flows.

Antall fig./tegn. større enn A4: 0 = fig./tegn.nr.:

Technical Note

To:	Norges Vassdrags- og Energidirektorat
From:	NGI
Date:	18th May, 2012
Document no.:	20110112-00-1-TN
Project:	Analyse av sedimentkolonnemetoden ift. karakterisering av sedimentenes avsetningsegenskaper
Author(s):	Dieter Issler (NGI and Intl. Centre for Geohazards) Tómas Jóhannesson (Veðurstófa Íslands, Reykjavík, Iceland)
Project leader:	Kalle Kronholm
Quality control:	Peter Gauer

Main office:
Pb. 3930 Ullevål Stadion
0806 Oslo, Norway

Trondheim office:
Pb. 1230 Pirsenteret
7462 Trondheim, Norway

Ph +47 22 02 30 00
Fax +47 22 23 04 48

Acct. no. 5096 05 01281
Org. no. 958 254 318 MVA

ngi@ngi.no
www.ngi.no

Dynamical Consistency Constraints on Entrainment and Deposition in Depth-Averaged Models of Snow Avalanches and Other Gravity Mass Flows

Contents

BS EN ISO 9001
Certified by BSI
Reg. no. FS 32989

Abstract

This paper discusses several issues related to the mathematical and physical formulation of entrainment in depth-averaged models of gravity mass flows (GMF) such as snow avalanches and landslides. (i) The relation between system boundaries, boundary conditions and entrainment-related source terms in the momentum balance and the equation of motion is clarified for different types of GMFs occurring in nature. (ii) Continuous deposition from a GMF requires that the bed exerts a larger shear stress than the interior of the flow can sustain. This is shown to imply that a GMF cannot accelerate due to deposition, contrary to some claims in the literature. (iii) Entrainment and deposition differ with respect to the boundary condition for the shear stress at the bed. (iv) The entrainment rate depends on the instantaneous flow conditions, the bed properties and the GMF rheology and thus cannot be specified independently of the latter. More specific results are obtained by limiting attention to basal erosion and assuming perfectly brittle behavior of the bed, characterized by its shear strength τ_c. For sliding block models, a simple explicit expression for the entrainment rate is derived in terms of the bed friction law and τ_c. For a quasi-stationary, uniform flow of a Bingham fluid over a brittle bed, the erosion rate and the modified velocity and shear-stress profiles are obtained analytically. Although the model cannot directly be applied to GMFs, entrainment rates consistent with estimates from field measurements are obtained for parameter values typical of snow avalanches. An extension of the theory to non-stationary flows and more general rheologies is proposed, but numerical studies will be needed to assess the accuracy of the approximations involved.

1 Introduction

Entrainment of ambient fluid or bed material has long been recognized as an important process in many types of gravity mass flows (GMFs). For example, field studies of snow avalanches (Issler et al., 1996; Sovilla et al., 2001) revealed that the moving mass may increase by an order of magnitude over the mass released initially. Interesting recent studies of granular flows (Barbolini et al., 2005) and snow avalanches (Sovilla, 2004) have begun to shed some light on the erosion and entrainment mechanisms. This experimental work has motivated new attempts at modeling entrainment in dense flows (Sovilla and Bartelt, 2002; Sovilla, 2004; Sailer et al., 2002; Naaim et al., 2004; Cherepanov and Esparragoza, 2008). Some of these models are based on Russian work from the 1960s to 1980s, where entrainment at the front or along the bottom of the flow was modeled by invoking an analogy either with shocks in gas dynamics (Briukhanov et al., 1967; Grigorian and Ostroumov, 1977) or with the theory of mixing at the interface in a stratified flow (Eglit, 1983). Other recent models that treat the GMF as a granular flow are inspired by Boutreux et al. (1998).

We address four key problems in this paper:

1. How is entrainment or deposition reflected in the momentum balance of depth-averaged GMF models?
2. What boundary conditions should be postulated?
3. Is deposition simply the reverse of entrainment?
4. Are there general consistency constraints on entrainment models?

The first point gave rise to an instructive debate whether an extra term is needed in the momentum balance to prevent the flow from accelerating due to deposition (Cannon and Savage, 1988; Hungr, 1990; Cannon and Savage, 1990; Erlichson, 1991). Some recent papers (Sovilla and Bartelt, 2002; Naaim et al., 2004) argued for a decelerating "entrainment force" in the momentum balance equation,

$$\sigma_e \equiv -q_e \bar{u}, \tag{1}$$

where q_e is the entrainment rate and $\bar{u}$ the depth-averaged velocity. However, this term is absent in the above-mentioned Russian analyses and some other recent papers (Sovilla et al., 2007) and computational models such as MN2D (Mohamed Naaim, pers. comm., 2007). Determining the correct formulation of the momentum equations is by no means an academic pastime: Mean entrainment rates $q_e = \mathcal{O}(50\,\mathrm{kg\,m^{-2}\,s^{-1}})$ at mean velocities around $50\,\mathrm{m\,s^{-1}}$ in large snow avalanches (Gauer and Issler, 2004) would mean an entrainment traction of $-2.5\,\mathrm{kPa}$, which is of the same order as the gravitational traction

$$\sigma_g \equiv (\bar{\rho}_f - \rho_a) g h \sin\theta \tag{2}$$

for typical avalanche tracks; estimates based on observations of debris flows lead to similar conclusions. $\bar{\rho}_f$ is the depth-averaged flow density, ρ_a the density of the ambient fluid, g the gravitational constant and θ the local slope angle. We will call stresses acting at the bed–flow interface "traction" in this paper, for lack of a better term; tractions or stresses divided by the flow density will be denoted with a caret henceforth. The key to determining the correct form of the momentum balance equation is precise definition of the system boundaries and imposing mathematically consistent and physically reasonable boundary conditions on the velocity and the stress. In Sec. 2, we propose simple boundary conditions that should be suitable for many rapid or very rapid GMFs. This discussion is a prerequisite for settling the mentioned dispute whether a flow can accelerate as a consequence of deposition.

Eglit and Demidov (2005) applied a variety of empirical entrainment parameterizations from different areas of application to an idealized snow avalanche and found the run-out distance and velocity to depend but weakly on the choice of parameterization. At first sight, this seems to imply that the fourth question above is irrelevant. However, their result may well be a consequence of assuming a rather small mobilizable mass. On physical grounds, the entrainment rate should be determined uniquely by the rheology of the flow (or the bed friction law) and the properties of the bed material. We investigate this for two types of models. The first type, which we call sliding-slab models, is characterized by a uniform velocity profile and a friction law implementing a slip boundary condition at the bed interface; the Voellmy, PCM and Savage–Hutter models belong to this category (Sec. 4). The second type comprises depth-averaged models with specified rheology that allows to compute the velocity profile, at least for steady flows. We analytically solve an idealized steady-flow situation of an entraining Bingham fluid in Sec. 5 and discuss an additional principle that can be invoked to extend this toy model to non-stationary flows in Sec. 6.

Entrainment and deposition are complex phenomena that manifest themselves in many different ways. It does, therefore, not seem possible to capture them comprehensively with one simple model. In order to make progress, we focus on selected aspects in this paper: First, we consider basal erosion only and disregard frontal plowing even though the latter mechanism may often be dominant, e.g., in wet-snow avalanches as well as in many debris flows or dry-snow avalanches (Sovilla, 2004). Second, we adopt a fluid-mechanical approach and explore constraints arising from inertia, in contrast to many geotechnically inspired attempts that derive erosion rates from stability considerations of the bed. Indeed, a central assumption in the second part of this paper is that the bed behaves as a perfectly brittle material with a well-defined shear strength τ_c. However, if the shear stress exceeds that value at the bed–flow interface, the bed should fail throughout its entire depth because the shear stress increases with depth. We defer a detailed study of this question to future work and postulate for the time being that the strength equals τ_c at the instantaneous interface to the flow and increases at a

sufficient rate with depth.

Much of our work is inspired by experience gained from studying snow avalanches, and our comparisons of estimated entrainment rates with observed ones refer to snow avalanches, where presently the best experimental information is available. However, our results in the first part (Secs. 2–3) are applicable to many types of eroding or depositing GMFs. The results presented in Secs. 4–6 depend strongly on the assumption or idealisation that the bed material is brittle and fails incrementally at the bed–flow interface, and it needs to be determined to which degree bed materials in other types of GMFs can be described in this way.

2 System boundaries, boundary conditions, and the difference between erosion and deposition

The shear stress that a fluid or particulate flow exerts on an erodible bed may exceed the binding strength of the bed particles. The breaking of the bonds is a rapid process (treated as instantaneous here) that we will call *erosion*, following the terminology of Gauer and Issler (2004). We reserve the term *entrainment* for the process that accelerates the eroded bed material and mixes it into the flow. Erosion may occur either locally and intermittently (inside turbulent eddies or during impact of particularly energetic particles) if the mean shear stress is below the bed shear strength, or quasi-continuously over large areas otherwise. In the first case (comprising, e.g., river flows), we call the flow *erosion-limited*, in the second case *entrainment-limited*. GMFs may fall into either category, depending on the flow and bed conditions.

There is often some arbitrariness in drawing the boundary between flow layers in multi-layered flows, but the choice made has consequences when formulating the balance equations. For example, high-speed videos of granular flows over granular beds (M. Barbolini and M. Pagliardi, personal communication, 2005) or of mudflows over a muddy bed (H. Breien and M. Pagliardi, personal communication, 2006) show that the bed may be set into slow shearing motion before erosion and entrainment occur or even if entrainment does not occur at all. If one considers a bed particle eroded and part of the flow as soon as its velocity differs from zero, eroded particles do not add momentum to the flow. Alternatively, if one considers the particle to become part of the flow only after it has been completely ripped out of the bed texture, the velocity at erosion is non-zero and erosion is accompanied by a particle-borne momentum flow from the bed to the current. While the bed shear can usually be neglected, the velocity at the interface of, e.g., a submarine debris flow and the turbidity current riding on it is non-zero, and the momentum exchange connected with mass exchange cannot be neglected.

A different situation is encountered in sand and snow drift: Particles in the salta-

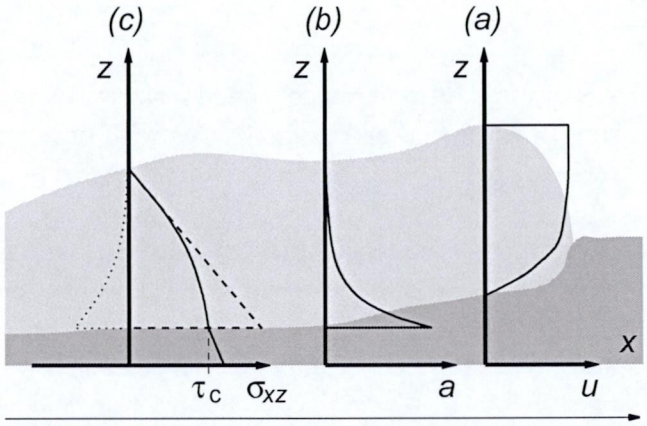

Figure 1. Schematic representation of a quasi-stationary gravity mass flow over an erodible bed. The interface shown is that between bed particles at rest and flow or bed particles in motion. (a) Qualitative velocity profile. (b) Qualitative acceleration profile. (c) Qualitative shear stress profile, showing the (integrated) contributions due to the weight of the flowing material (dashed line) and the inertial pseudo-force from the acceleration of the eroded bed material (dotted line). The resulting net shear stress (full line) tends to the threshold value τ_c at the erosion interface.

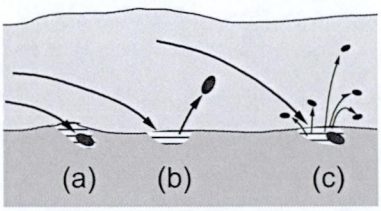

Figure 2. Schematic representation of the mass and momentum exchange processes between an erodible bed and a layer of saltating particles. Particles impacting on the bed may be absorbed (a) or rebound (b), and bed particles may be ejected with non-zero initial velocity as a result of the impact (c).

tion layer impact on the bed at velocities close to the mean flow velocity and may be absorbed by the bed (Fig. 2). The impact may also cause bed particles to be ejected with non-zero initial velocity. In either case, the mass exchanged across the interface also carries momentum. In the literature, the so-called grain-borne shear stress is therefore distinguished from the shear stress exerted by the ambient fluid. Examples of the resulting momentum balance equations can be found in (Issler, 1998; Issler et al., 2000; Gauer, 2001).

Many presently used dynamic models assume shear to be concentrated in a thin bottom layer, which is then idealized as a slip interface between the bed and the flow. The velocity profile of the flow is assumed uniform, $u_x(x, z, t) = \bar{u}_x(x, t)$ for $b(x, t) < z \leq s(x, t)$, where $b(x, t)$ and $s(x, t)$ are the instantaneous bottom

and top surfaces of the flow. If there is entrainment (or deposition), the velocity discontinuity at $z = b(x,t)$ requires a corresponding jump in the shear stress,

$$\Delta\sigma_{xz} \equiv \sigma_{xz}^{(b+)} - \sigma_{xz}^{(b-)}, \tag{3}$$

where the superscript $(b_\pm)$ means that the stress is evaluated at $z = b_\pm$, approaching the interface from above $(+)$ or below $(-)$. We will pursue the implications for the dynamics in Sec. 4 and stress here that the system boundary can be chosen either at b_- or b_+. At b_-, the eroded material enters the system with zero momentum and the boundary condition on the shear stress is $\sigma_{xz}^{(b-)}$, which must be determined by the physical properties of the bed material. If one chooses b_+, the entrained material adds momentum at a rate $q_e\bar{u}$ while the shear stress $\sigma_{xz}^{(b+)}$ is determined by the flow properties, which are summarized by the friction law in this type of model.

Lê and Pitman (2009) proposed an instructive variant on this theme to resolve the ambiguity in the choice of the system boundary by assuming a very thin but non-vanishing entrainment layer and identifying the system boundary with its middle. There they find $u_x^{(b)} = \bar{u}_x/2$ and correctly include the momentum flow across that boundary. This is an equally valid—and equally arbitrary—choice. We will briefly discuss the dynamical aspects of their model in Sec. 5.

In models with non-uniform velocity profile, there is no need for a slip velocity nor for a discontinuity in the shear stress. However, entrainment modifies the velocity profile: Eroded particles must be accelerated, which implies that a net force is acting on them and that the shear stress is reduced compared to the non-entraining case, especially near the bottom. Neglecting horizontal stress gradients, the momentum balance in the flow direction x at height z perpendicular to the bed yields

$$\sigma_{xz}(z) = \int_z^s \rho_f(g\sin\theta - D_t u_x)dz' < \bar{\rho}_f g(s-z)\sin\theta \tag{4}$$

since the material derivative $D_t u_x \equiv \partial_t u_x + \mathbf{u}\cdot\nabla u_x > 0$ in the bottom layer; see the schematic shear stress profiles in Fig. 1.

In order to determine the boundary condition on the shear stress, we consider flow materials for which the shear stress is an increasing function of the shear rate. In this case, there is a fundamental feedback mechanism: If the erosion rate is too small, the gravitational traction is not completely balanced by the bed shear stress and the inertial forces due to the acceleration of eroded material, hence the flow velocity will increase. By this, the shear stress increases and raises the erosion rate. Conversely, if the erosion rate is too large for entrainment to be sustained by the current shear stress, the flow is decelerated so that the bed shear stress and thus the erosion rate diminish.

By combining microscopic and macroscopic considerations, appropriate boundary conditions may be suggested: On average, a minimum shear stress (depending on the bed and flow materials) is needed to break a particle out of the bed

surface, $\sigma_{xz} \geq \tau_c$. Right after a particle has broken loose, a force arising from the shear stress gradient near the bed (cf. Fig. 1) acts on it and accelerates it. If the time required to break the inter-particle bonds is much shorter than the time required to move the particle through the layer near the bottom with a high shear stress gradient, the erosion rate is limited by the entrainment process. Accordingly, the erosion rate attains the largest value that leaves the bed shear stress at its threshold value τ_c. This is expected to be the case for materials that exhibit brittle behavior at the particle scale, among them snow or weakly cohesive sands under the action of rapid flows. Only if the bed material is very ductile so that breaking it requires relatively long time and large deformations, will the supply of eroded particles be too low to diminish the bed shear stress to its minimum value. We conclude that for many if not most rapid gravity mass flows, the required boundary condition is

$$\sigma_{xz}(x, b(x,t), t) \approx \tau_c. \tag{5}$$

Owen (1964) used very similar reasoning in the context of sand and snow drift.

Evidently, Eq. (5) represents a simplification in that fluctuations in the shear stress exerted by the flow will allow limited erosion to occur for mean shear stresses below τ_c. Also, τ_c may depend on the loading rate and thus on the details of the fluctuation spectrum of the flow. In general, it is to be expected that there is a significant spatial and temporal variability in the value of τ_c. In subaerial debris flows, the soil type will usually vary along the path as well as the degree of water saturation, which is moreover a strong function of time. In snow avalanches, the snow properties vary significantly between avalanche occurrences in the same path, and they vary both on the large scale (e.g., due to temperature differences of up to 10° C between the release area and the run-out zone of large avalanches and strong winds at high altitudes) and the small scale (differing expositions to the wind and the sun). In many situations, τ_c will moreover show pronounced dependence on the depth within the erodible bed. In the following, we will explore the consequences of the simplest case, namely Eq. (5), and assume that the spatial variability of τ_c will be taken into account in practical applications as appropriate.

In models with slip boundary conditions, the condition (5) applies at $z = b_-(x,t)$. The shear stress at $z = b_+(x,t)$ is given by the friction law specific to the model. However, one should expect that entrainment modifies the friction law because, from a micro-mechanical point of view, the interface in reality consists of one or several layers of particles that are being accelerated. Hence, the relative velocity between the slab and the uppermost particle layer in the interface is significantly smaller than the slab velocity.

While the fundamental condition for erosion to occur is that the flow exerts a shear stress exceeding the strength of the bed material, deposition will only occur if the bed is able to exert a larger shear stress than the flowing material can

sustain internally. Otherwise, the bed friction would merely cause the entire flow to decelerate and eventually stop. Deposition, in contrast, is the process where the flow velocity changes but slowly while the bed arrests particles from the bottom layer of the flow. This condition on the shear stress is not in itself sufficient; it is equally necessary that the arrested particles immediately become part of the bed and assume its properties, in particular the higher strength compared to the flowing material. Rapid sintering under pressure, as is known to occur in snow, is a candidate mechanism. The near absence of shear in the bed is probably a prerequisite for sintering to occur, as may be the presence of sufficiently large roughness elements to hold the stopped particles in place while sintering progresses. Observations from dry-snow or powder-snow avalanches suggest a variant of this mechanism where large particles from the fluidized flow impact the snow cover surface in a nearly ballistic fashion and get stuck in the impact crater they produce (Issler et al., 1996, P. Gauer, personal comm. 2006).

Considering the intricacies of the deposition process, we conjecture that in many cases deposits found in the path of GMFs represent the stopped tail of the flow rather than material from the bottom of the main body. For example, high-speed video recordings of subaerial and subaqueous laboratory mudflows show how the tail of the flow is immobilized when the flow depth falls below a limiting value that is related to the yield strength of the slurry. Such flow behavior can be described adequately (except in point-mass models) without invoking any deposition model. In contrast, gradual settling-out of particles (often accompanied by normal grading of the deposits), as is observed in powder-snow avalanches, turbidity currents and sandy debris flows, can be considered deposition.

In most cases it will not be possible to state the stress boundary conditions for deposition as simply as Eq. (5) because the maximum stress sustained by the flow is expected to depend on the flow velocity. In a cohesionless granular assembly, $\sigma_{xz}^{(b-)}$ and $\sigma_{xz}^{(b+)}$ may be tentatively related to the static and dynamic friction angle, respectively:

$$\sigma_{xz}^{(b-)} \approx \sigma_{zz}^{(b)} \tan\phi_{\text{stat}} \quad \text{and} \quad \sigma_{xz}^{(b+)} \approx \sigma_{zz}^{(b)} \tan\phi_{\text{dyn}}. \tag{6}$$

Can deposition cause the flowing mass to accelerate? This question was raised by Hungr (1990), who noted the similarity of the model proposed by Cannon and Savage (1988) with the equations for rocket motion. The center-of-mass equation of motion of the GMF, $d(mv)/dt = F_{\text{ext}}$, can be written as

$$m\frac{dv}{dt} = F_g - F_f - \frac{dm}{dt}v. \tag{7}$$

F_g is the component of the gravitational force along the path, F_f the bed friction and v the velocity. The flow accelerates if $v\,dm/dt < F_g - F_f$ or, equivalently, $vq_e < \sigma_g - \sigma_{xz}^{(b)}$, with q_e taking negative values for deposition, and $\sigma_g \equiv \bar{\rho}gh\sin\theta$. Indeed, this equation is the same as the rocket equation in a variable gravitational

field $(F_g - F_f)/m(t)$ if the combustion rate is identified with the deposition rate and the exhaust speed relative to the rocket were always exactly equal to the rocket speed $v(t)$. The challengers of applying Eq. (7) to GMFs argued that it must be wrong because it would allow a GMF to accelerate like a rocket even if $F_f > F_g$, provided it sheds enough mass.

In order to demonstrate intuitively why Eq. (7) is indeed correct but lacks a constraint, we idealize the GMF as a solid block sliding over an abrasive surface. We may distinguish a top domain with mass M per unit area and velocity V and a thin bottom domain with mass m per unit area and velocity v. The thickness of the bottom domain is chosen such that it corresponds to the material abraded within the time interval Δt, coming to rest from its initial velocity V. Each domain is subjected to gravity, and the abrasion layer additionally to the bed shear stress $\sigma_{xz}^{(b)} \equiv \sigma_b$. The shear stress at the interface between the layers is designated by $\sigma_{xz}^{(i)} \equiv \sigma_i$. The equations of motion for the two layers are

$$M\Delta V/\Delta t = Mg\sin\theta - \sigma_i, \tag{8}$$

$$m\,\Delta v/\Delta t = mg\sin\theta + \sigma_i - \sigma_b. \tag{9}$$

According to the assumptions, $\Delta v = -V$, and $m/\Delta t = q_d$ is the abrasion or deposition rate. Letting $\Delta t \to 0$, which implies $m \to 0$, we obtain

$$M\dot{V} = Mg\sin\theta - \sigma_i, \tag{10}$$

$$m\dot{v} = -q_d V = \sigma_i - \sigma_b > -\sigma_b \tag{11}$$

if $\sigma_i > 0$, which is the case since the internal stresses must be dissipative in a frictional flow. Note that $mg\sin\theta \to 0$ as $\Delta t \to 0$, but $m\dot{v}$ tends to the finite value $\sigma_i - \sigma_b < 0$ if the sliding block is abraded. We will return to this point in Sec. 4. The motion of the top domain is determined by the shear stress transmitted inside the material, and there is no unphysical acceleration. When we add the two equations, Eq. (7) results, which is essentially the equation used by Cannon and Savage and is also correct for deposition. It has to be supplemented, however, by the condition that the bed must exert a larger shear stress on the bottom domain than can be transmitted inside the block itself. If this condition is not met, deposition or abrasion is not possible. The abrasion rate is governed by the difference between the bed shear stress and the internal shear stress near the bed. Equation (11) implies a (loose) upper limit on the deposition rate q_d, which is sufficient to prevent unphysical acceleration. The same arguments can be applied to GMFs behaving as fluids.

3 Momentum balance and equation of motion with entrainment

In a depth-averaged formulation of a gravity-driven mass flowing over an erodible bed, entrainment or deposition are described by means of mass and momentum fluxes through the bottom layer boundary (and also the top boundary

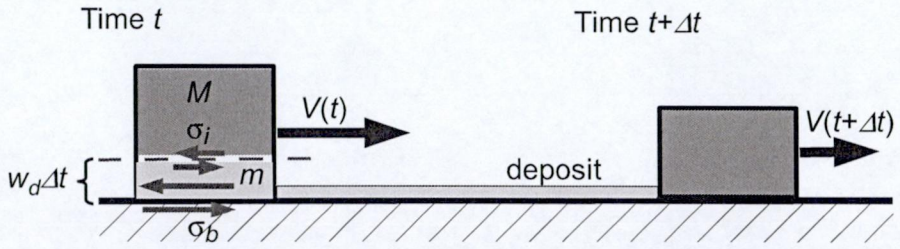

Figure 3. Block sliding over abrasive plane. w_d: abrasion speed, σ_b: shear sress exerted by ground, σ_i: maximum shear stress sustained within block.

in the case of multi-layered flows). The flow is divided into slices of infinitesimal length Δx that extend over the entire depth of the layer (Fig. 4; we limit ourselves to the two-dimensional case for simplicity of notation). In the Euler representation, the boundaries 1 and 3 are fixed, i. e., their velocities $\mathbf{w}_{1,3} = \mathbf{0}$. The boundaries 2 and 4 are moving with velocities

$$\mathbf{w}_2(x,t) = \hat{\mathbf{k}}\partial_t b(x,t), \quad \mathbf{w}_4(x,t) = \hat{\mathbf{k}}\partial_t s(x,t) \tag{12}$$

expressed in terms of the functions $b(x,t)$ and $s(x,t)$ describing the location of the interfaces. The orthonormal basis vectors $\hat{\mathbf{i}}$, $\hat{\mathbf{k}}$ are defined as tangent and normal to the slope, respectively. (If the slope angle is variable, additional terms related to the curvature arise, but we disregard this complication here. For a treatment of these geometrical effects see e. g. (Eglit, 1983; Savage and Hutter, 1991; Gray et al., 1999).) The conservation equations for mass and momentum, integrated over the slice, are

$$\frac{d}{dt}\int_V dV\,\rho + \oint_{\partial V} dA\,\rho(\mathbf{u}-\mathbf{w})\cdot\hat{\mathbf{n}} = 0, \tag{13}$$

$$\begin{aligned}\frac{d}{dt}\int_V dV\,\rho\mathbf{u} + \oint_{\partial V} dA\,\rho\mathbf{u}(\mathbf{u}-\mathbf{w})\cdot\hat{\mathbf{n}} \\ = \int_V dV\,\rho\mathbf{g} + \oint_{\partial V} dA\,\sigma\cdot\hat{\mathbf{n}}.\end{aligned} \tag{14}$$

Several authors have detailed the correct evaluation of these integrals, most recently Tai and Kuo (2008), who treat a rather general case with entrainment and time-varying curvilinear coordinates. Therefore we do not repeat this derivation in detail here, but concentrate on the interpretation and application of their results.

The volume integrals do not pose any difficulty; density-weighted averaging is used for $\mathbf{u}$. The surface integrals are decomposed into terms associated with the boundaries 1 to 4, see Figure 4. The integration over the boundaries 2 and 4 takes into account their movement, Eq. (12), and their lengths, $\sqrt{1+(\partial_x b)^2}\Delta x$ and $\sqrt{1+(\partial_x s)^2}\Delta x$, respectively. The fields ρ, $\mathbf{u}$ and σ may be discontinuous

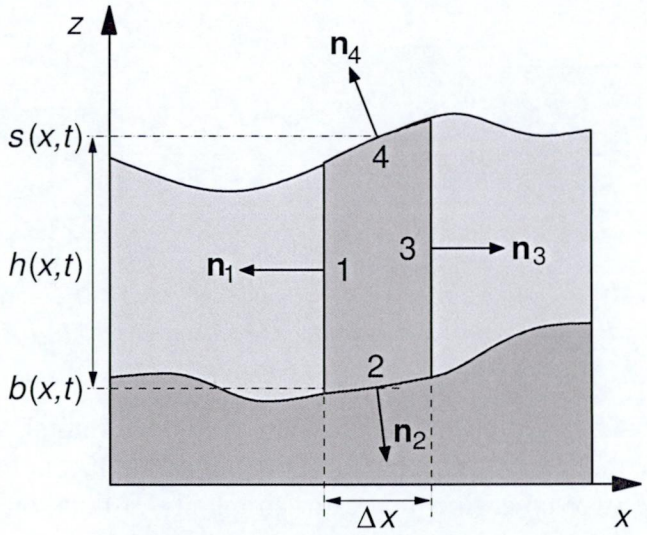

Figure 4. Definition sketch of the integration volume used in the derivation of the mass and momentum balance equations in the presence of bed entrainment (or deposition to the bed).

at the boundaries 2 and 4 so that the jump conditions

$$[\![\rho(\mathbf{u}-\mathbf{w})\cdot\hat{\mathbf{n}}]\!] = 0, \tag{15}$$

$$[\![\rho\mathbf{u}(\mathbf{u}-\mathbf{w})\cdot\hat{\mathbf{n}}]\!] = [\![\sigma\cdot\hat{\mathbf{n}}]\!] \tag{16}$$

have to be used to ensure mass and momentum conservation; here

$$[\![f(z=b)]\!] \equiv f(b_+) - f(b_-) \quad \text{with} \quad b_+ \searrow b,\ b_- \nearrow b \tag{17}$$

and analogously at $z = s(x,t)$.

Letting $\Delta x \to 0$ in the depth-integrated mass balance equation, one obtains

$$\partial_t(h\bar{\rho}) + \partial_x(h\bar{\rho}\,\bar{u}_x) = q_b - q_s \equiv q_e, \tag{18}$$

where q_b, q_s and q_e are the bed entrainment rate, the suspension rate from the top surface, and the total entrainment rate, respectively, which can take both positive and negative values. The bed entrainment rate is evaluated as

$$q_b = \rho^{(b_+)}\left(u_z^{(b_+)} - u_x^{(b_+)}\partial_x b - \partial_t b\right), \tag{19}$$

which reduces to $q_b = -\rho^{(b_-)}\partial_t b$ by virtue of the jump condition (15) if the bed material is at rest. The suspension rate,

$$q_s = \rho^{(s_+)}\left(u_z^{(s_+)} - u_x^{(s_+)}\partial_x s - \partial_t s\right), \tag{20}$$

vanishes identically if the well-known kinematic boundary condition of a material surface applies.

A corresponding calculation for the x-component of the momentum balance equation, again using Eq. (16), results in two alternative formulations, which coincide if velocity and shear stress are continuous at the bed interface:

$$\begin{aligned} &\partial_t(h\bar{\rho}\,\bar{u}_x) + \partial_x\left(h\bar{\rho}\,\overline{u_x^2}\right) - h\bar{\rho}\,g\sin\theta - h\partial_x\bar{\sigma}_{xx} \\ &= \sigma_{xz}^{(s+)} - \sigma_{xz}^{(b-)} - q_s u_x^{(s+)} + q_b u_x^{(b-)} \qquad (21) \\ &= \sigma_{xz}^{(s-)} - \sigma_{xz}^{(b+)} - q_s u_x^{(s-)} + q_b u_x^{(b+)} \qquad (22) \end{aligned}$$

If the bed is at rest and the flow is eroding, $\sigma_{xz}^{(b-)} \approx \tau_c$ and $u_x^{(b-)} = 0$ according to Sec. 2, thus there is neither momentum influx nor outflux due to entrainment, and the bed shear stress is locked at τ_c as long as entrainment occurs. If deposition and entrainment are due to particle impact and splashing (or to turbulent suspension), the grain-borne momentum exchange between the flow and the bed is taken into account by the last two terms in Eqs. (21) and (22).

It is instructive to convert the momentum-balance (21) or (22) to the equivalent equation of motion by substituting the mass balance (18) into it, assuming that $\bar{\rho} = \text{const.}$ in the flow and that there is no shear stress at the upper surface. Using the advective derivative $D_t \equiv \partial_t + \bar{u}_x\partial_x$, the result is

$$\begin{aligned} D_t\bar{u}_x &= g\sin\theta + \frac{1}{h\bar{\rho}}\left[h\partial_x\bar{\sigma}_{xx} - \sigma_{xz}^{(b)}\right] \\ &\quad -\frac{1}{h}\partial_x\left[h\left(\overline{u_x^2} - \bar{u}_x^2\right)\right] \qquad (23) \\ &\quad -\frac{1}{h\bar{\rho}}\left(q_e\bar{u}_x + q_s u_x^{(s)} - q_b u_x^{(b)}\right). \end{aligned}$$

When applying this equation to models with slip boundary conditions, the appropriate limits $b_\pm$, $s_\pm$ have to be substituted for b and s. The second line vanishes if the velocity profile is uniform, and is small in most cases. This equation of motion indeed features an entrainment pseudo-force (the last term), which is equivalent to a retarding stress $-q_e\bar{u}_x$ in case of entrainment ($q_e > 0$) if the interface velocities are zero. It is the reaction to the force exerted by the flow onto the eroded particles that have to be accelerated to the speed $\bar{u}_x$ through mixing. It may be noted that the effect of entrainment on the momentum balance of the flow in Eq. (21) is identical to the effect of entrained water from the melting of ice from englacial tunnel walls on the momentum balance of sudden outburst floods from glaciers, which are called jökulhlaups (Spring and Hutter, 1981, Eq. (2.2)).

4 Entrainment in sliding slab models with slip boundary condition

In sliding-slab models, the velocity profile is assumed to be uniform, $u_x(z) = u_p$, with a discontinuity at the bed interface. If there is entrainment and the stress boundary condition $\sigma_{xz}^{(b)} \approx \tau_c$, discussed in the preceding section, is adopted, the velocity discontinuity at $z = b$ requires a discontinuity in the shear stress so that an infinitesimally small amount of mass can be accelerated from rest to a finite velocity within an infinitesimally small time interval. A simple-minded derivation of the entrainment rate proceeds as follows: The shear stress immediately below the interface is $\sigma_{xz}^{(b-)} \approx \tau_c$, while its value right above the interface is given by the friction law:

$$\sigma_{xz}^{(b+)} = \bar{\rho}_f f(u_p, h, \ldots). \tag{24}$$

The jump in the shear stress across the interface is responsible for accelerating the eroded particles to the speed u_p, thus the entrainment rate should be

$$q_e = \frac{\bar{\rho}_f f(\ldots) - \tau_c}{|u_p|} \quad \text{if} \quad \bar{\rho}_f f(\ldots) > \tau_c. \tag{25}$$

The weak point in the derivation presented above is that several physical quantities could develop discontinuities across the interface that might combine to produce effects that are not taken into account in Eq. (25). We address this point by considering the dynamics of a thin shear layer, with thickness d that we will let tend to zero in the end. Similar reasoning was used recently by Lê and Pitman (2009), who assumed that the rheology of the shear layer was given by the Jenkins and Savage (1983) theory for rapid granular flows of nearly elastic uniform spheres. Lê and Pitman were, however, only interested in the mean velocity in the middle of the layer and did not pursue the dynamical implications for entrainment, since they assumed a heuristic equation for the entrainment rate from the outset.

The boundary conditions at the top and bottom of the shear layer are

$$\begin{aligned} u(0,t) &= 0, \qquad u(d,t) = u_p(t), \\ \hat{\sigma}_{xz}(0,t) &= \hat{\tau}_c, \quad \hat{\sigma}_{xz}(d,t) = f(u_p(t), h(t)). \end{aligned} \tag{26}$$

u_p is the velocity of the plug layer ($z \geq d$) riding on top of the entrainment layer. At the interfaces $z = 0$ and $z = d$, the velocity and shear stress are continuous while the shear rate jumps from 0 to $\dot{\gamma}(0_+, t)$ at $z = 0$ and from $\dot{\gamma}(d_-, t)$ to 0 at $z = d$.

The mass balance equation is trivially satisfied in the shear layer with $d = \text{const.}$, the material having a uniform bed-normal velocity $u_z(x, z, t) = w_e(t)$ and x-independent longitudinal velocity $u_x(z, t)$ in the coordinate system that moves in the slope-normal direction with the erosion front. The equation of motion in the flow direction is

$$D_t u_x = g \sin\theta + \partial_z \hat{\sigma}_{xz}, \tag{27}$$

where the material derivative $D_t \equiv \partial_t + u_x\partial_x + u_z\partial_z$ simplifies to $\partial_t + w_e\partial_z$ in our case. The left-hand side of Eq. (27) thus becomes $w_e\dot{\gamma}(z,t) + \partial_t u_x(z,t)$. As we let the shear-layer thickness tend to zero, $\dot{\gamma}$ increases without bounds so that $\partial_t u_x$ (stemming from the acceleration of the slab) and $g\sin\theta$ (arising from the weight of the material in the shear layer) can be neglected. Equation (27) may now be formulated as

$$w_e\dot{\gamma} = \partial_z\hat{\sigma}_{xz}. \tag{28}$$

This result does not depend on the particular rheology and is exact if the flow is stationary. Integration of Eq. (28) across the shear layer then gives

$$w_e u_p = \hat{\sigma}_{xz}(d) - \hat{\sigma}_{xz}(0) = f(u_p, h) - \hat{\tau}_c, \tag{29}$$

which leads directly to Eq. (25). We will use the above analysis as our starting point in Sec. 5.

Formula (25) applies both in equilibrium and non-equilibrium situations. Neglecting longitudinal gradients in h, the acceleration of the plug flow,

$$D_t u_p = g\sin\theta - \frac{f(u_p, h, \ldots)}{h}, \tag{30}$$

is the same as if there were no entrainment, i.e., if τ_c were larger than the actual friction. The last term on the right-hand side is interpreted as the sum of the decelerations $-\hat{\tau}_c/h$ (frictional traction) and $-q_e u_p/(h\bar{\rho}_f)$ (acceleration of eroded bed material).

Figure 5 shows the shape of the entrainment rate function for, respectively, a pure Coulomb friction law ($\sigma_{xz} = \sigma_{zz}\tan\delta$, with bed friction angle δ as in the

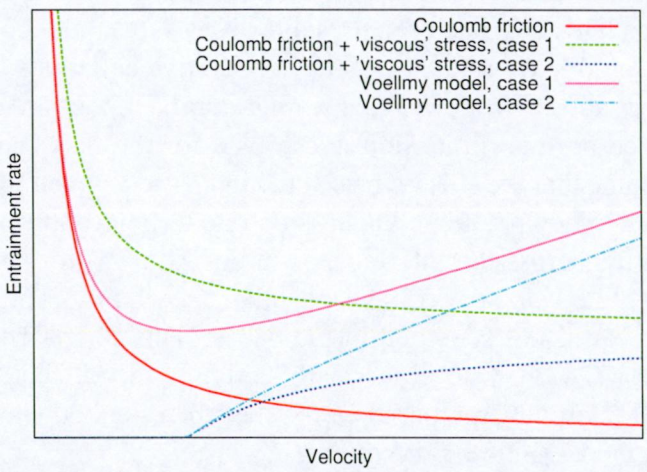

Figure 5. Qualitative velocity dependence of the entrainment rate for flows with slip boundary condition at the bed, uniform velocity inside the flow and different friction laws, in arbitrary units. Cases 1 and 2 refer to the shear stress at $u = 0$ being larger or smaller, respectively, than the bed shear strength.

Savage–Hutter model), Coulomb friction combined with linear 'viscous' friction ($\sigma_{xz} = \sigma_{zz} \tan\delta + k_1 u_p$), and the Voellmy or Perla–Cheng–McClung (PCM) model ($\sigma_{xz} = \sigma_{zz} \tan\delta + k_2 \rho u_p^2$). Completely different high-velocity behavior results for the different friction laws. Another noteworthy feature is the divergence of the entrainment rate as $u_p \to 0$ if the shear stress remains larger than the bed shear strength in this limit.

If one assumes (i) that the flow material has a characteristic strength $\tau_f < \tau_c$ above which it no longer deforms in a controlled way, but breaks apart or is abraded, (ii) that the friction on the bed can exceed this threshold, and (iii) that the bed is able to rapidly bond stopped flow material, the deposition rate can be determined in the same way as the erosion rate (25):

$$q_d = \frac{\bar{\rho}_f f(\ldots) - \tau_f}{|u_p|} \quad \text{if} \quad \tau_f < \bar{\rho}_f f(\ldots) < \tau_c. \tag{31}$$

As already mentioned in Sec. 2, it is to be expected from micro-mechanical considerations that the friction traction is changed by the entrainment process itself. The function $f(\ldots)$ in Eqs. (25) and (31) is the one appropriate for entrainment/deposition, but lack of knowledge will usually force one to replace it by the one without entrainment.

It is instructive to compare the results obtained in this section to some of the entrainment models proposed in the literature:

One can beg the question of the correct formulation of the entrainment term by resolving the bed-normal dimension instead of depth-averaging. This is carried out most completely by e.g. Crosta et al. (2009), who model the stresses, not only in the flow, but also in the bed and thus do not need to make assumptions about the erosion rate. This approach requires, however, substantial computational resources and a suitable formulation of the constitutive equations before and after failure. Bovet et al. (2010) envisage a similar approach, but present simulations in which the bed-normal dimension is resolved for the flow only. Like in this paper, they assume that the shear stress at the interface is given by the strength of the bed material. They postulate the erosion rate to be proportional to the jump of the shear stress across the interface, as in our Eq. (25) for sliding-slab models, even though the velocity profile is calculated explicitly. The proportionality constant is, however, not specified in the paper. This differs from the work of Issler and Pastor (2011), who numerically compute the velocity profile and the entrainment rate without free parameters other than the bed shear strength in a 1-dimensional model (in the z-direction).

The majority of the existing depth-averaged models with entrainment use the same friction law as in the case without entrainment and do not include the entrainment traction in the *momentum balance equation*. In the formulation (21) with the system boundary at $b_-(x,t)$, this is equivalent to not adopting our pro-

posed boundary condition (5). In the alternative formulation (22) with the system boundary at $b_+(x,t)$, this amounts to neglecting the momentum carried into the flow by the already accelerated eroded material. With all other elements of the model equal, our boundary conditions would lead to higher flow velocities.

The "entrainment traction" $-q_b\bar{u}_x$ in the momentum balance equations proposed by Sovilla and Bartelt (2002) and Naaim et al. (2004) is opposite in sign to our result (in the formulation (22) with the system boundary at b_+). These models would therefore predict significantly lower velocities and lower entrainment rates than ours. Later versions of these models (e.g., (Sovilla et al., 2007), Naaim, pers. comm. 200?) omit the "entrainment force" term.

Tai and Kuo (2008) correctly obtain an equation corresponding to Eq. (21) or (22). In order to arrive at a sliding-slab type model, they implicitly choose the formulation with the boundary at b_+ by using $u_x^{(b+)} = \bar{u}_x$, assuming a uniform velocity profile. They use the frictional traction as given by their friction law, corresponding to its value at b_+, and take into account the momentum influx $q_e\bar{u}_x$. Specifying an entrainment rate different from Eq. (25), as they do, amounts to postulating a stress boundary condition that differs from our proposal.

In the two-layer powder-snow avalanche model by Issler (1998), bed friction is the result of momentum exchange due to particle absorption, rebounding and ejection. The concept of an essentially constant bed shear stress does not apply in this context dominated by particle impacts. At the interface between the saltation and suspension layers, velocity and stress are continuous and the momentum exchange rate is proportional to the mass exchange rate.

Generally, the published models use their specific friction law for non-entraining flows, $\sigma_f = \bar{\rho}_f\tilde{f}(\ldots)$, together with some heuristic entrainment rate function $\tilde{q}_e(\ldots)$ that differs from Eq. (25). This could be interpreted in our framework in terms of a variable bed shear strength $\tau_c = \bar{\rho}_f\tilde{f}(\ldots)$ and an effective friction law in the presence of entrainment, $f_{\text{eff.}}(\ldots) = \tilde{f}(\ldots) + \tilde{q}_e(\ldots)|u_p|/\bar{\rho}_f$.

5 Relation between the entrainment rate and the velocity profile in quasi-steady flow

In order to study the subtle interplay between the shear stresses and the entrainment or deposition rate, let us build a toy model, using a hypothetic material that behaves as a solid with a shear strength τ_c, above which it disintegrates into a cohesive granular fluid with a yield strength $\tau_y < \tau_c$ and (Bingham) kinematic viscosity ν:

$$\dot{\gamma}(z) = \partial_z u_x = \begin{cases} 0, & |\sigma_{xz}| \le \tau_y; \\ \operatorname{sgn}(\sigma_{xz})\frac{|\sigma_{xz}|-\tau_y}{\rho_f\nu}, & |\sigma_{xz}| \ge \tau_y. \end{cases} \tag{32}$$

In order to concentrate on the essential points and to obtain analytic solutions, we consider an infinitely extended slope with inclination θ, on which an infinitely long sheet of depth h (measured perpendicular to the slope) flows at constant speed. This assumption eliminates the gradients of the longitudinal normal stress and momentum flux. We further postulate that the eroded bed material is immediately replenished from below so that the interface between bed and flow is inclined at the same angle θ. Also, let material be removed from the top of the flow (without application of shear stresses) at the same rate as it is entrained from below so that the total flow depth and the plug-layer depth remain constant. Under these conditions, a steady flow is possible and the flowing material has a constant velocity component $w_e = u_z = q/\rho_f$ normal to the bed; momentum is taken away from the system at the rate $-\rho_f u_x(h) w_e$.

The plug-layer extends from the surface of the flow to a height r above the bed:

$$r = h - \frac{\hat{\tau}_y}{g \sin\theta}. \tag{33}$$

In the absence of entrainment, the shear stress profile would be linear,

$$\hat{\sigma}_{xz}^{(0)}(z) = g(h - z)\sin\theta, \tag{34}$$

the shear rate would diminish linearly from the bed to the height r,

$$\dot{\gamma}^{(0)}(z) = \begin{cases} \frac{g(r-z)\sin\theta}{\nu}, & z \le r; \\ 0, & z \ge r, \end{cases} \tag{35}$$

and the velocity profile would be parabolic in the shear layer if there is no sliding at the bed,

$$u_x^{(0)}(z) = \begin{cases} \frac{g\sin\theta}{2\nu}\left(2rz - z^2\right), & z \le r; \\ \frac{g\sin\theta}{2\nu} r^2, & z \ge r. \end{cases} \tag{36}$$

With entrainment in our idealized situation, the velocity profile will remain constant in time, but deviate from Eq. (36).

The equation of motion for a fluid element results from Eq. (27) with $D_t u_x = w_e \dot{\gamma}$ as in the derivation of Eq. (28) by substituting for $\partial_z \hat{\sigma}_{xz}$:

$$\frac{d\dot{\gamma}}{dz}(z) - \frac{w_e}{\nu}\dot{\gamma}(z) = -\frac{g\sin\theta}{\nu}, \quad 0 \le z \le r. \tag{37}$$

The boundary condition $\dot{\gamma}(r) = 0$ leads to the solution

$$\dot{\gamma}(z) = \begin{cases} \frac{g\sin\theta}{w_e}\left(1 - e^{-\frac{w_e}{\nu}(r-z)}\right), & 0 \le z \le r; \\ 0 & r \le z \le h, \end{cases} \tag{38}$$

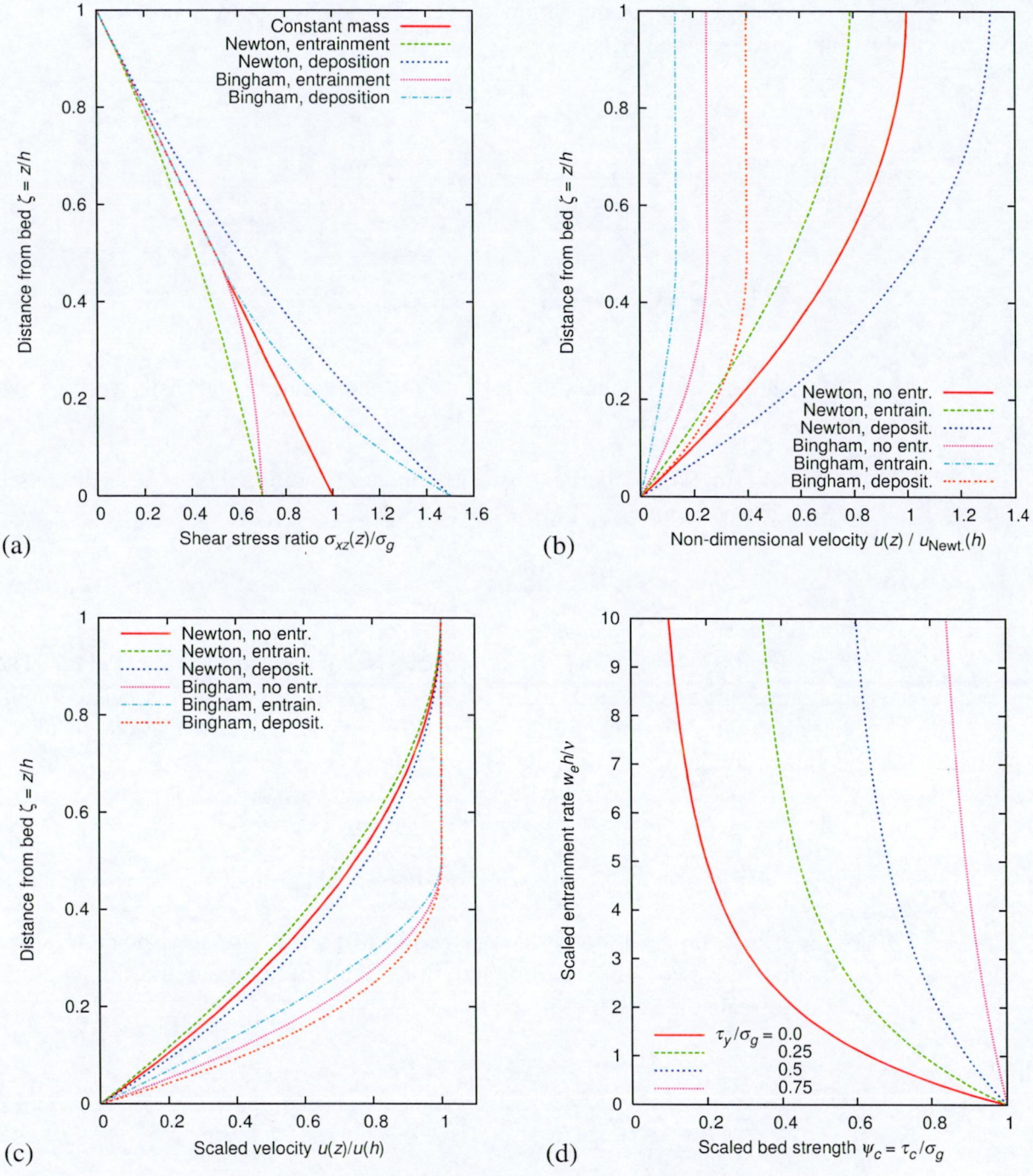

Figure 6. Non-dimensionalized profiles of (a) shear-stress and (b) velocity for stationary flows of Newtonian and Bingham fluids on an inclined plane, with and without entrainment or deposition. The parameter values are $\varsigma = 0.5$ for the Bingham fluid, $\psi_c = \tau_c/\sigma_g = 0.7$ for the entraining flows, and $\sigma_{xz}(0)/\sigma_g = 1.5$ for the depositing flows. (c) Velocity profiles for non-entraining, entraining and depositing Newtonian and Bingham fluids, scaled with their surface velocity. The same parameter values are used as in Fig. 6. (d) Dependence of the entrainment rate on the bed shear strength τ_c for various values of the yield strength τ_y of the Bingham fluid. All quantities are non-dimensionalized according to Eq. (43).

from which we obtain the following velocity and shear-stress profiles if we assume no slip at the bed:

$$u_x(z) = \begin{cases} \frac{g\sin\theta}{w_e}\left[z - \frac{\nu}{w_e}\left(e^{-\frac{w_e}{\nu}(r-z)} - e^{-\frac{w_e}{\nu}r}\right)\right], & 0 \le z \le r; \\ \frac{g\sin\theta}{w_e}\left[r - \frac{\nu}{w_e}\left(1 - e^{-\frac{w_e}{\nu}r}\right)\right], & r \le z \le h, \end{cases} \tag{39}$$

$$\hat{\sigma}_{xz}(z) = \begin{cases} \hat{\tau}_y + \frac{\nu g\sin\theta}{w_e}\left(1 - e^{-\frac{w_e}{\nu}(r-z)}\right), & 0 \le z \le r; \\ g(h-z)\sin\theta, & r \le z \le h. \end{cases} \tag{40}$$

By expanding the exponential functions to second order, one easily verifies that Eqs. (38)–(40) reduce to Eqs. (34)–(36) in the limit $w_e \to 0$.

Subjecting Eq. (40) to the shear-stress boundary condition $\hat{\sigma}_{xz}^{(b)} = \hat{\tau}_c$, as discussed in Sec. 2, we obtain

$$\frac{\nu g\sin\theta}{w_e}\left(1 - e^{-\frac{w_e r}{\nu}}\right) = \hat{\tau}_c - \hat{\tau}_y. \tag{41}$$

In the limit $\tau_y \to 0$, $r \to h$, an eroding Newtonian fluid is recovered. The equation is transcendental and must be solved for w_e by numerical methods. Note, however, that integration of Eq. (28) from 0 to h and application of the boundary conditions leads to the simple relation

$$w_e u(h) = \hat{\sigma}_g - \hat{\tau}_c, \tag{42}$$

with $\hat{\sigma}_g = hg\sin\theta$, as is to be expected on physical grounds.

In order to compare the steady-state profiles of shear stresses, shear rates and velocities in Newtonian and Bingham fluids with and without entrainment, it is useful to scale the variables in the following way:

$$\begin{aligned} &\zeta = z/h, && \psi = \sigma_{xz}/\sigma_g, && \psi_y = \tau_y/\sigma_g, \\ &\upsilon = \frac{u_x}{\frac{gh^2\sin\theta}{2\nu}}, && \varsigma = \frac{r}{h} = 1 - \psi_y, && \chi = \frac{w_e}{\nu/h}, \end{aligned} \tag{43}$$

where $\sigma_g = \rho_f g h \sin\theta$ will be called "gravitational traction" in the following. The expressions obtained after scaling are listed in Table 1, and Fig. 6.b shows the scaled velocity profiles for selected parameter values. In order to highlight the differences in the shapes of the velocity profiles, they are rescaled by the respective maximum velocity in Fig. 6.c.

In depth-averaged models, we can obtain a first-order approximation and circumvent the expensive evaluation of a non-linear equation for each grid cell and at each timestep by using the velocity profiles of non-entraining flows even with

Table 1. Vertical profiles of shear stress and longitudinal velocity in steady-state flows of Newtonian and Bingham fluids with and without entrainment. All quantities are non-dimensionalized according to Eq. (43). In the limit of vanishing entrainment, i. e. $\chi \to 0$, all profiles with entrainment reduce to the corresponding profiles without entrainment. The Boussinesq form factor $f \equiv h\int_0^h u^2 dz / \left(\int_0^h u dz\right)^2$ is evaluated for $\varsigma = 0.5$ for the Bingham fluid and for $\psi = 0.7$ in the case of entrainment. The values of χ indicated in brackets correspond to physically consistent entrainment rates.

	Interval	Shear-stress profile $\psi(\zeta)$	Velocity profile $v(\zeta)$	Boussinesq form factor f
Newtonian fluid, no entrainment	$[0,1]$	$1-\zeta$	$2\zeta-\zeta^2$	1.20
Newtonian fluid, entrainment	$[0,1]$	$\frac{1}{\chi}\left(1-e^{-\chi(1-\zeta)}\right)$	$\frac{2}{\chi}\left[\zeta-\frac{1}{\chi}\left(e^{-\chi(1-\zeta)}-e^{-\chi}\right)\right]$	1.22 ($\chi=0.76$)
Bingham fluid, no entrainment	$[0,\varsigma]$	$1-\zeta$	$2\varsigma\zeta-\zeta^2$	1.10
	$[\varsigma,1]$		ς^2	
Bingham fluid, entrainment	$[0,\varsigma]$	$1-\varsigma+\frac{1}{\chi}\left(1-e^{-\chi(\varsigma-\zeta)}\right)$	$\frac{2}{\chi}\left[\zeta-\frac{1}{\chi}\left(e^{-\chi(\varsigma-\zeta)}-e^{-\chi\varsigma}\right)\right]$	1.11 ($\chi=4.46$)
	$[\varsigma,1]$	$1-\zeta$	$\frac{2}{\chi}\left[\varsigma-\frac{1}{\chi}\left(1-e^{-\chi\varsigma}\right)\right]$	

entrainment or deposition. Combining eqs. (42), (32) and (36) with the bottom boundary condition for the shear stress, one arrives at

$$\chi \approx \frac{2}{\varsigma}\cdot\frac{1-\psi_c}{\psi_c-\psi_y}, \tag{44}$$

$$v(1) \approx \varsigma\cdot(\psi_c-\psi_y). \tag{45}$$

The Boussinesq form factor (which appears in the momentum balance) changes only by a small amount as long as dynamically sustainable entrainment rates are specified, see the last column of Table 1. However, the relative error in the entrainment rate and velocity increases rapidly with increasing entrainment rate, i.e., with decreasing ratio $(\tau_c-\tau_y)/\sigma_g$. In the case $\psi_c = 0.7$, $\psi_y = 0.5$ (implying $\varsigma = 0.5$), the approximation yields $\chi \approx 6.0$ and $v(1) \approx 0.1$, whereas the self-consistent solution is $\chi = 4.46$ and $v(1) = 0.134$.

Comparison of the predicted entrainment rates with experimental data is difficult because erosion rates have rarely been measured, and then mostly in dry-snow avalanches (Gauer and Issler, 2004; Sovilla, 2004) for which a Bingham fluid is a

Table 2. Examples of entrainment rates obtained for different combinations of snowcover strength (τ_c), yield strength (τ_y) and Bingham viscosity (ν_B) in the flow. Idealized stationary flow with constant density 200 kg m^{-3}, flow height 1 m and surface velocity 20 m s^{-1} at slope angle 30°.

τ_c [Pa]	τ_y [Pa]	ν_B [m^2 s^{-1}]	w_e [m s^{-1}]	q_e [kg m^{-2} s^{-1}]
700	500	0.0168	0.075	15.0
800	600	0.0125	0.050	10.0
800	300	0.0489	0.050	10.0
900	600	0.0165	0.025	5.0

poor approximation. Nevertheless, assuming typical values such as a slope angle of 30°, a flow depth of 1 m, a density of 200 kg m^{-3} and a surface velocity of 20 m s^{-1}, we obtain the values listed in Table 2 for several internally consistent combinations of τ_c, τ_y and ν_B, which are of the right order of magnitude.

Most entrainment models specify the entrainment rate as a function of either $\sigma_g - \tau_c$ or $\bar{u}$ (Eglit and Demidov, 2005). For the present proposal, Eq. (41) shows w_e to depend on $\tau_c - \tau_y$, θ, g, ν and—through the shear-layer depth r—on h. Even though the equation cannot be solved for, e.g., $w_e(h)$, keeping the other parameters fixed, w_e and h can be expressed as functions of $\chi = w_e h/\nu$ and plotted (Fig. 7, bottom panel). Similarly, the surface velocity and h can be expressed through χ (top panel). It is also possible to solve for w_e in terms of $u^{(s)}$ using suitable algebraic manipulations, but it would be misleading to consider this as the velocity dependence of the entrainment rate because the velocity is a dependent variable in this setting: Choosing u at will with given θ, ν, τ_c and τ_y determines the unique flow height that realizes this value of u.

The present method can be straightforwardly extended to non-linear rheologies. However, the differential equation corresponding to (37) becomes non-linear and will in general defy analytic solution. Accordingly, no closed (even if transcendental) equation can be formulated for the entrainment rate in terms of the threshold shear stress. This circumstance severely limits the practical applicability of the approach unless a simple yet sufficiently accurate parametrization of the profile function can be found such that q_e can be obtained by solving a single equation for each grid node and timestep. Even though the general condition (42) together with the rheological equation and the bed stress boundary condition $\sigma_b = \tau_c$ provide an approximate solution, its accuracy cannot be assessed without solving the full problem.

The solution for the entrainment rate obtained for sliding-slab models in Sec. 4 cannot be recovered from the present model as the limit $\hat{\tau}_y \to hg \sin\theta$ and $\nu \sim$

$(hg\sin\theta - \hat{\tau}_y)^\alpha$ for some suitably chosen exponent α. The reason is that $\hat{\sigma}_b = \hat{\tau}_c < \hat{\tau}_y$ is required in this limit, whereas the shear stress increases monotonically with depth in the Bingham model and thus necessarily $\tau_y < \tau_c$. Only if one admits different rheologies in the plug layer and the shear layer can a solution be found with $\tau_y > \tau_c$.

To conclude this section and illustrate the similarities and differences between deposition and entrainment, we modify our toy model, supplying material at the top at surface velocity and removing it at the bottom after it has come to rest. Deposition makes the non-dimensionalized shear stress profile (cf. Fig. 6.a) convex instead of concave in the shear layer; the value at the bed interface exceeds the gravitational traction. Similarly, the velocity normalized by its value at the surface is larger in the shear layer than in the flow without deposition, opposite to the effect of entrainment (see Fig. 6.c). In contrast to the eroding flow, the material properties do not impose a boundary condition for the bottom shear stress in the depositing flow. The rate at which mass is supplied to the flow at its surface speed determines the flow velocity according to Eq. (39), with negative w_d instead of positive w_e. We stress, however, that determination of the deposition rate in more realistic situations requires explicit modeling of the flow dynamics and consolidation processes at the bed–flow interface, which cannot be carried out strictly within the framework of depth-averaged equations.

6 Extension to non-stationary flows

The value of the toy model discussed above consists in its analytic solvability that allows us to analyze all aspects in detail. It has four features that are not realistic in the context of GMFs, namely (i) it neglects frontal entrainment and variations of flow properties in the streamwise direction, (ii) it is restricted to Bingham-type rheologies, (iii) it requires mass to be continually removed from the system to keep the flow depth constant, and (iv) the flow is assumed quasi-stationary. A numerical approach addressing problems (ii) and (iii) is proposed by Issler and Pastor (2011). We may anticipate that the fundamental relation (42) is modified substantially: First, if mass is not artificially removed from the top, the eroded mass only needs to be accelerated to the depth-averaged velocity $\overline{u}_x$ instead of the surface velocity $u_x(h)$. Second, the difference between gravitational traction and bed shear strength is reduced or enhanced by inertial forces as the flow accelerates or decelerates.

In the present paper, we investigate approximations that allow us to address problem (iv) by analytical methods. The essential problem can be highlighted by writing the force balance for a slice inside the flow as

$$\sigma_e + \sigma_i + \sigma_b = \sigma_g + h\partial_x\bar{\sigma}_{xx}, \tag{46}$$

where σ_g is the gravitational traction $\rho gh\sin\theta$ and $\sigma_i = \overline{\rho}hD_t\overline{u}$ is the inertial

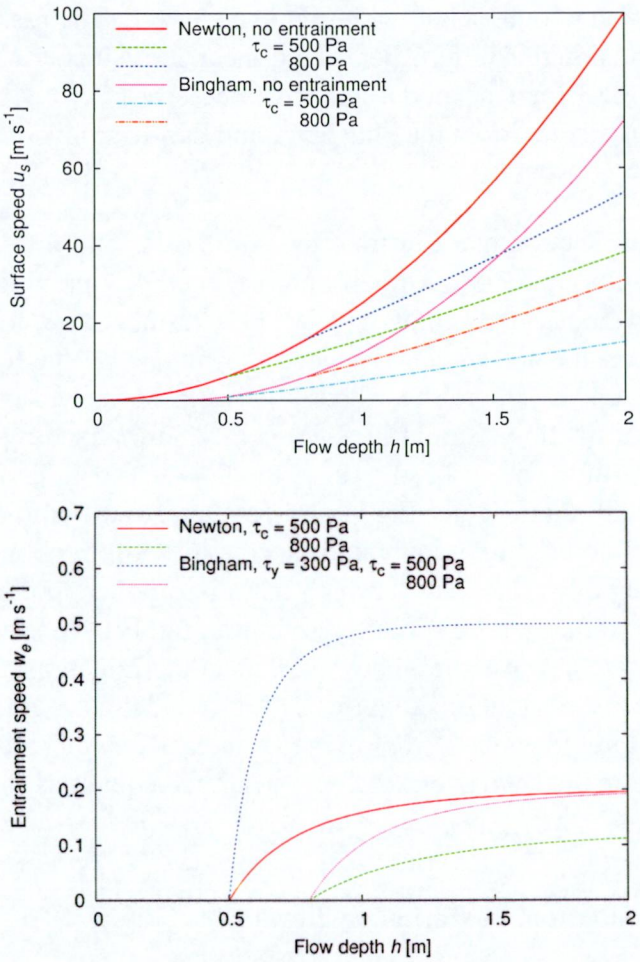

Figure 7. Dependence of the surface flow velocity u_s (top panel) and entrainment speed w_e (bottom panel) on the total flow depth h for (quasi-)stationary Newtonian and Bingham fluids with and without entrainment. A slope angle of 30°, a flow density of 200 kg m^{-3} and a viscosity of 0.1 m^2 s^{-1} are assumed.

force per unit length of flow. The right-hand side of (46) is known at each stage of the calculation, hence the problem consists in (i) determining the value of the bed shear stress, and (ii) apportioning the available traction $\sigma_g - \sigma_b + h\partial_x\bar{\sigma}_{xx}$ between acceleration of the flow (σ_i) and entrainment ($\sigma_e \equiv q_e u_x(h)$).

The arguments why the bed shear stress should be equal to the bed shear strength, $\sigma_{xz}^{(b)} = \tau_c$, essentially carry over to non-stationary flows. One should expect that the bed shear stress will fluctuate somewhat in reality, but for the purpose of modeling it should be sufficient to use τ_c as an estimate of its mean value.

On physical grounds, it is clear that the entrainment rate must be determined by the unknown instantaneous shear stress profile near the bed–flow interface. If we boldly approximate the shape of the non-stationary velocity profile by the shape of the quasi-stationary one, we conclude that *the instantaneous entrainment rate*

in the non-stationary case is (approximately) the same as in a stationary flow with equal bed shear strength, flow height and depth-averaged flow velocity. However, the slope angle θ_s on which the corresponding stationary flow would develop is different from the slope angle θ of our non-stationary flow. This proposal may be formulated mathematically as

$$w_e^{(\mathrm{ns})} \approx w_e^{(\mathrm{s})}(\bar{u})|_{\bar{u}=\bar{u}^{(\mathrm{ns})}}; \tag{47}$$

superscripts (s) and (ns) denote the stationary flow with slope angle θ_s and the original non-stationary flow with slope angle θ, respectively. Once w_e is known, the acceleration of the flow can be determined from

$$\sigma_i = \sigma_g - \tau_c + h\partial_x\bar{\sigma}_{xx} - \rho w_e \bar{u}. \tag{48}$$

We emphasize, however, that numerical tools are needed to assess the error induced by this approximation.

Applying this approach to a Bingham fluid, we first note that the depth of the shear layer, r_s, is determined by the gravitational acceleration minus the acceleration of the plug layer, a_p, which is not known a priori. Within the plug layer, the resulting shear stress is the same as the one due to gravity on a different slope with inclination θ_s:

$$\hat{\sigma}_{xz}(z,t) = (h-z)(g\sin\theta - a_p) = (h-z)g\sin\theta_s. \tag{49}$$

The non-dimensionalized shear-layer depth then results as

$$\varsigma_s \equiv \frac{r_s}{h} = 1 - \frac{\hat{\tau}_y}{gh\sin\theta_s} = 1 - \frac{\psi_y}{p}, \tag{50}$$

where

$$p \equiv \frac{\sin\theta_s}{\sin\theta}. \tag{51}$$

Now assume that the velocity profile has the same shape, given in Table 1, as in a quasi-stationary entraining flow of a Bingham fluid with the same flow depth h and instantaneous shear-layer depth r_s, given by Eq. (50). Through the constitutive equation, the velocity profile determines the vertical shear stress profile. An approximate vertical profile of acceleration can also be calculated from the approximate instantaneous velocity profile and the rates of change of $\bar{u}_x$ and r_s. There will, in general, be an inconsistency when the approximate vertical profiles of acceleration, velocity and shear stress are used in the momentum balance equation (the local form of Eq. (14)), but we proceed assuming that the error is tolerably small.

The equations for the bed shear stress and the surface velocity can be obtained from Eqs. (41) and (39) by substituting θ_s for θ ($\partial_x(h\bar{\sigma}_{xx}) = 0$ for our example) and non-dimensionalizing with respect to the Newtonian surface velocity $gh^2\sin\theta/(2\nu)$ and gravitational traction $\rho gh\sin\theta$ at the *true* slope angle θ:

$$p\cdot\frac{1}{\chi}\left(1 - e^{-\varsigma_s\chi}\right) = \psi_c - \psi_y, \tag{52}$$

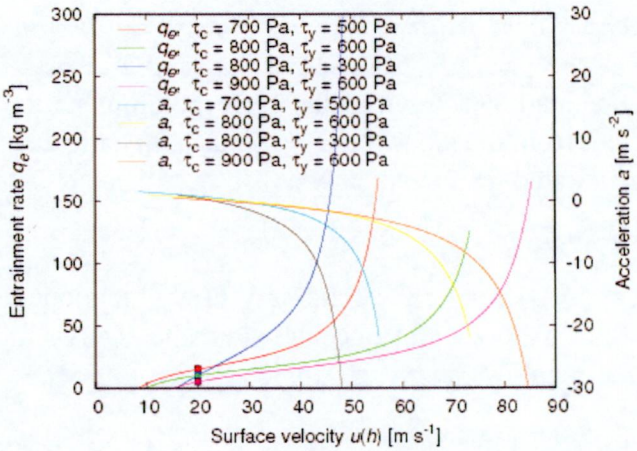

Figure 8. Velocity dependence of the entrainment rate q_e (left axis) and acceleration a (right axis) on the surface velocity of a Bingham fluid according to the approximate extended model. The flow height is held constant at 1 m, the slope angle is 30° and the density 200 kg m^{-3}. The colored squares represent the entrainment rate values from the exact quasi-stationary equation, listed in Table 2.

$$p \cdot \frac{2}{\chi}\left[\varsigma_s - \frac{1}{\chi}\left(1 - e^{-\varsigma_s \chi}\right)\right] = \upsilon(1). \tag{53}$$

Dividing both equations by p and substituting (52) in (53) results in

$$\frac{2}{\chi}\left(1 - \frac{\psi_c}{p}\right) = \frac{\upsilon(1)}{p}. \tag{54}$$

In terms of χ and known quantities, p is thus given by

$$p = \frac{1}{2}\upsilon(1)\chi + \psi_c. \tag{55}$$

This we insert back into (52), using (55) in (50):

$$\left(\frac{\upsilon(1)}{2} + \frac{\psi_c}{\chi}\right)\left(1 - e^{-\chi + \frac{\psi_y}{\upsilon(1)/2 + \psi_c/\chi}}\right) = \psi_c - \psi_y. \tag{56}$$

Once χ is known, (55) is used again to obtain p. The acceleration of the flow (with $D_t \equiv \partial_t + \bar{u}_x \partial_x$ in this context) is given by

$$h D_t \bar{u}_x = \hat{\sigma}_i = \hat{\sigma}_g(1 - p) = hg(\sin\theta - \sin\theta_s). \tag{57}$$

As in the case of the quasi-stationary flow discussed earlier, the instantaneous local entrainment rate can be obtained by solving a non-linear equation. However, in addition to the bed and flow material parameters, ψ_c, ψ_y and ν, the non-equilibrium flow velocity now also appears as a parameter in the equation. By

inserting the quasi-stationary value, $v(1) = (1/\chi)[\varsigma_s - (1/\chi)(1 - \exp(-\varsigma_s\chi))]$, one verifies that (56) is equivalent to Eq. (41) in the quasi-stationary case. Figure 8 shows the result of numerically solving the approximate equations for the entrainment rate and the acceleration as a function of the surface velocity in the case of the flows whose quasi-stationary solutions are given in Table 2. The extended approximate model reproduces the exact quasi-stationary solutions quite well.

Two features are notable: (i) There is an effective threshold velocity below which erosion ceases, and (ii) $q_e(u(h))$ diverges at some value of $u(h)$. Taking the limit $\chi \to \infty$ in Eq. (56) shows immediately that $v_{\max} = 2(\psi_c - \psi_y)$ in this approximate model, and this is confirmed by the numerical solution plotted in Fig. 8. However, the divergence of χ is an unphysical artifact of our approximations. Furthermore, expanding Eq. (56) around $\chi = 0$, one finds that positive solutions for χ exist only if

$$v(1) > \frac{(\psi_c - \psi_y)^2}{\psi_c}, \tag{58}$$

which is again confirmed by the numerical solution. Note that negative solutions cannot simply be interpreted as deposition because the boundary conditions implemented in Eq. (56) no longer apply, cf. the discussion in Sec. 2. The condition (58) is physical: At the threshold for entrainment, the depth-averaged flow acceleration is $\bar{a} = (g \sin\theta - \hat{\tau}_c)/h$. We approximate the plug-layer acceleration by $a_p \approx \bar{a}$ and obtain the depth of the shear layer at erosion threshold as

$$h_s = h - \frac{\hat{\tau}_y}{g \sin\theta - a_p} \approx h \cdot \left(1 - \frac{\hat{\tau}_y}{\hat{\tau}_c}\right) = h\left(1 - \frac{\psi_y}{\psi_c}\right). \tag{59}$$

The bed shear stress becomes $\hat{\sigma}_{xz}^{(b)} = \hat{\tau}_y + \nu\frac{2u_p}{h_s}$. As this must be equal to $\hat{\tau}_c$, we again obtain the condition (58) upon non-dimensionalization according to Eq. (43).

7 Conclusions and outlook

The main results of this investigation may be summarized as follows:

1. Depending on the precise definition of the system boundaries in a flow with entrainment of ambient fluid or bed material, different formulations of the momentum balance may be obtained that need to be interpreted consistently. In the case of entrainment from a bed at rest without splashing, the most natural system definition leaves no "entrainment force" term in the momentum balance equation, but there is a significant retarding term $-q\bar{\mathbf{u}}$ in the equation of motion. Entrainment from moving ambient fluid or due to splashing requires a momentum source term $q\mathbf{u}\,|_{\text{interface}}$ in the momentum balance and a corresponding term in the equation of motion.

2. Contrary to claims in the literature, the equations presented here do not allow a flow to accelerate due to strong deposition because the internal shear stresses in the flow limit the deposition rate.

3. For a class of materials characterizable by brittle fracture at an erosion threshold stress τ_c, the erosion and entrainment behavior is determined by the boundary condition that the shear stress at the bed–flow interface should be equal to τ_c. Several flows of geophysical importance—among them snow and rock avalanches, perhaps also debris flows—are expected to be adequately described in this way.

4. Entraining and deposition modify the velocity and shear stress profiles of GMFs due to the gradual acceleration/deceleration of the entrained/deposited mass. The difference is expected to be small in most practical applications, however. In the case of entrainment of brittle bed material, we argued that the erosion rate tends to the value that makes the interfacial shear stress equal to the erosion threshold. Deposition depends on additional material properties that control the consolidation of the deposited material.

5. When using heuristic parameterizations of the entrainment rate, they need to be chosen to be consistent with the rheology or the friction law of the flow. In general, only a complete, non-averaged analysis will produce a fully consistent solution, but we presented a simple solution for plug-like models with a friction law describing the basal shear stress.

6. A practically important class of eroding flows are those limited by their entrainment capacity rather than by their erosive capacity. Our analysis in Sec. 5 shows how to determine the entrainment rate in the case of quasi-stationary flow of a Bingham fluid. Extension of this approach to other rheologies is possible in principle, but contingent on the availability of (at least approximate) closed-form solutions to the profile equations.

7. We give physical arguments for a criterion that allows extension of our method to non-stationary flows if the velocity and shear-stress profiles remain self-similar. The velocity dependence of the entrainment rate can then be determined approximately. Further work is needed to elucidate the range of applicability of the scheme.

The following general issues need to be considered in more detail to make this theory fully applicable in computational models: (i) How can deviations of the velocity profile from its non-entrainment equilibrium shape be parameterized in a simple way applicable in one- and two-dimensional depth-averaged flow models? (ii) How rapidly do the velocity and shear-stress profiles adapt themselves to changed conditions, e. g. at slope breaks or due to variability of the bed material? (iii) How well can the erosion behavior of specific bed materials be described by a single threshold shear stress? (iv) How does the threshold shear stress depend on other, more easily measurable parameters of a given material?

The first question can be studied by searching for analytic solutions to simplified flow situations like the one assumed in Sec. 5. Of particular interest are expressions for rheologies other than Bingham and for situations where the flow depth is allowed to grow in proportion with the entrained mass and the velocity increases accordingly. In contrast, the second problem can be effectively studied by numerically solving the evolution equation of the velocity profile in a simplified, but non-stationary situation, e.g., after a sudden slope break and neglecting longitudinal stress gradients. This results in a one-dimensional evolution equation. Its solutions will hopefully suggest useful parameterizations of the transient velocity profile for use in depth-averaged models.

The third question requires dedicated experimental work, mainly in the laboratory along the lines indicated by Barbolini et al. (2005). The goal of measuring the erosion rate as well as the density, velocity and shear stress profiles with sufficient accuracy to test Eq. (5) represents a major experimental challenge, however. The fourth problem will also require experimental work, the methods of which will have to be adapted to the specific properties of the material to be studied.

The scope of this paper was deliberately narrowed to just one mechanism of entrainment, namely continuous erosion along the bottom of the flow. In many situations of practical interest, entrainment at the front is of similar importance or even dominant. Many of the general results from the first three sections also apply to frontal entrainment, but a different approach is needed for modeling the front resistance, plowing depth and front shape. The recent paper by Cherepanov and Esparragoza (2008) approaches the problem with concepts from fracture mechanics, making assumptions that are in many ways opposite to ours: They neglect inertial forces near the erosion front, which are crucial in our model, but they stress the role of fracture energy, which we neglect by assuming perfectly brittle behavior. The two approaches should not be considered conflicting but complementary, focusing on two different zones of the bed–flow interface where different entrainment mechanisms dominate. One of the challenges ahead is to merge both concepts into a unified description of entrainment based on the relevant physical processes.

Acknowledgments

Much of this work was funded by the EU 5th Framework Programme through the project SATSIE (EU Contract no. EVG1–CT2002–00059) and by the Swiss National Science Foundation (grant no. 200021–101911). In the final phase, support for DI came from the project SafeLand in the EU 7th Framework Programme (EU Contract no. 226479), from the Research Council of Norway through grant 181709, "Snow avalanche research", a special internal grant from NGI, and a fellowship from the NILS Mobility Project (ABEL Extraordinary Chair action). We are grateful to Massimiliano Barbolini, Margarita E. Eglit, Peter

Gauer, Carl B. Harbitz and Mohamed Naaim for fruitful and enjoyable discussions that encouraged us to write this paper. DI also thanks Manuel Pastor Pérez and his group at CEDEX in Madrid for their hospitality and interest during the final write-up. This is paper no. XYZ from the International Centre for Geohazards.

Bibliography

Barbolini, M., A. Biancardi, F. Cappabianca, L. Natale, and M. Pagliardi (2005), Experimental study of erosion processes in snow avalanches, *Cold Regions Sci. Technol.*, **43**(1–2), 1–9; doi:10.1016/j.coldregions.2005.01.007.

Boutreux, T., E. Raphaël, and P.-G. de Gennes (1998), Surface flows of granular materials: A modified picture for thick avalanches, *Phys. Rev. E*, **58**, 4692–4700.

Bovet, E., B. Chiaia and L. Preziosi (2010), A new model for snow avalanche dynamics based on non-Newtonian fluids, *Meccanica*, **45**(6), 753–765; doi:10.1007/s11012-009-9278-z.

Briukhanov, A. V., S. S. Grigorian, S. M. Miagkov, M. Y. Plam, I. Y. Shurova, M. E. Eglit, and Y. L. Yakimov (1967), On some new approaches to the dynamics of snow avalanches, in *Physics of Snow and Ice, Proc. Intl. Conf. Low Temperature Science, Sapporo, Japan, 1966. Vol. I, Part 2*, edited by H. Ôura, pp. 1223–1241, Institute of Low Temperature Science, Hokkaido University, Sapporo, Hokkaido, Japan.

Cannon, S. H., and W. Z. Savage (1988), A mass-change model for the estimation of debris-flow runout, *J. Geol.*, **96**, 221–227.

Cannon, S. H., and W. Z. Savage (1990), A mass-change model for the estimation of debris-flow runout: A reply, *J. Geol.*, **98**, 792.

Cherepanov, G. P., and I. E. Esparragoza (2008), A fracture-entrainment model for snow avalanches, *J. Glaciol.*, **54**(184), 182–188.

Crosta, G. B., S. Imposimato, and D. Roddeman (2009), Numerical modelling of entrainment/deposition in rock and debris-avalanches, *Engng. Geol.*, **109**(1–2), 135–145; doi:10.1016/j.enggeo.2008.10.004.

Eglit, M. E. (1983), Some mathematical models of snow avalanches, in *Advances in the Mechanics and the Flow of Granular Materials*, vol. II, edited by M. Shahinpoor, 1st ed., pp. 577–588, Trans Tech Publications, Clausthal-Zellerfeld, Germany.

Eglit, M. E., and K. S. Demidov (2005), Mathematical modeling of snow entrainment in avalanche motion, *Cold Regions Sci. Technol.*, **43**(1–2), 10–23; doi:10.1016/j.coldregions.2005.03.005.

Erlichson, H. (1991), A mass-change model for the estimation of debris-flow runout, a second discussion: Conditions for the application of the rocket equa-

tion, *J. Geol.*, **99**, 633–634.

Gauer, P. (2001), Numerical modeling of blowing and drifting snow in Alpine terrain, *J. Glaciol.*, **47**(156), 97–110.

Gauer, P., and D. Issler (2004), Possible erosion mechanisms in snow avalanches, *Annals Glaciol.*, **38**, 384–392.

Gray, J. M. N. T., M. Wieland, and K. Hutter (1999), Gravity-driven free surface flow of granular avalanches over complex basal topography, *Proc. R. Soc. Lond. A*, **455**, 1841–1874.

Grigorian, S. S., and A. V. Ostroumov (1977), The mathematical model for slope processes of avalanche type (in Russian), Scientific Report 1955, Institute for Mechanics, Moscow State University, Moscow, Russia.

Hungr, O. (1990), A mass-change model for the estimation of debris-flow runout: A discussion, *J. Geol.*, **98**, 791.

Issler, D. (1998), Modelling of snow entrainment and deposition in powder-snow avalanches, *Annals Glaciol.*, **26**, 253–258.

Issler, D., P. Gauer, M. Schaer, and S. Keller (1996), Staublawinenereignisse im Winter 1995: Seewis (GR), Adelboden (BE) und Col du Pillon (VD), Internal Report 694, Eidg. Institut für Schnee- und Lawinenforschung, CH–7260 Weissfluhjoch/Davos, Switzerland.

Issler, D., P. Gauer, and M. Barbolini (2000), Continuum models of particle entrainment and deposition in snow drift and avalanche dynamics, in *Models of Continuum Mechanics in Analysis and Engineering. Proceedings of a conference held at the Technische Universität Darmstadt, September 30 to October 2, 1998*, edited by R. Balean, pp. 58–80, Shaker Verlag, Aachen, Germany.

Issler, D., and M. Pastor Pérez (2011), Numerical study of entrainment dynamics in various rheologies, *Annals Glaciol.*, **52**(58), 143–147.

Jenkins, J. T. and S. B. Savage (1983), A theory for the rapid flow of identical, smooth, nearly elastic, spherical particles, *J. Fluid Mech.*, **130**, 187–202.

Lê, L. and E. B. Pitman (2009), A model for granular flows over an erodible surface, *SIAM J. Appl. Math.*, **70**(5), 1407–1427; doi:10.1137/060677501.

Naaim, M., F. Naaim-Bouvet, T. Faug, and A. Bouchet (2004), Dense snow avalanche modeling: flow, erosion, deposition and obstacle effects, *Cold Regions Sci. Technol.*, **39**, 193–204.

Owen, P. R. (1964), Saltation of uniform grains in air, *J. Fluid Mech.*, **20**(2), 225–242.

Sailer, R., L. Rammer, and P. Sampl (2002), Recalculation of an artificially released avalanche with SAMOS and validation with measurements from a pulsed Doppler radar, *Nat. Hazards Earth Syst. Sci.*, **2**, 211–216.

Savage, S. B., and K. Hutter (1991), The dynamics of avalanches of granular material from initiation to runout. Part I: Analysis, *Acta Mechanica*, **86**, 201–223.

Sovilla, B. (2004), Field experiments and numerical modelling of mass entrain-

ment and deposition processes in snow avalanches, Ph.D. thesis, Swiss Federal Institute of Technology, CH–8092 Zürich, Switzerland.

Sovilla, B., and P. Bartelt (2002), Observations and modelling of snow avalanche entrainment, *Nat. Hazards Earth Syst. Sci.*, **2**, 169–179.

Sovilla, B., S. Margreth, and P. Bartelt (2007), On snow entrainment in avalanche dynamics calculations, *Cold Regions Sci. Technol.*, **47**(1–2), 69–79.

Sovilla, B., F. Sommavilla, and A. Tomaselli (2001), Measurements of mass balance in dense snow avalanche events, *Annals Glaciol.*, **32**, 230–236.

Spring, U., and K. Hutter (1981), Numerical studies of jökulhlaups, *Cold Regions Sci. Technol.*, **4**, 227–244.

Tai, Y. C., and C. Y. Kuo (2008), A new model of granular flows over general topography with erosion and deposition, *Acta Mech.*, **199**, 71–96.

Kontroll- og referanseside/ *Review and reference page*

NGI

Dokumentinformasjon/*Document information*

Dokumenttittel/*Document title*		Dokument nr/*Document No.*
Dynamical Consistency Constraints on Entrainment and Deposition in Depth-Averaged Models of Snow Avalanches and Other Gravity Mass Flows		20110112-00-1-TN
Dokumenttype/*Type of document*	**Distribusjon/*Distribution***	**Dato/*Date***
☐ Rapport/*Report*	☒ Fri/*Unlimited*	2012-05-18
☒ Teknisk notat/*Technical Note*	☐ Begrenset/*Limited*	**Rev.nr./*Rev.No.***
	☐ Ingen/*None*	0

Oppdragsgiver/*Client*
Norges vassdrags- og energidirektorat

Emneord/*Keywords*
Gravity mass flows, snow avalanches, mathematical modeling, bed entrainment

Stedfesting/*Geographical information*

Land, fylke/*Country, County*	Havområde/*Offshore area*
—	—
Kommune/*Municipality*	**Feltnavn/*Field name***
—	—
Sted/*Location*	**Sted/*Location***
—	—
Kartblad/*Map*	**Felt, blokknr./*Field, Block No.***
—	—

UTM-koordinater/*UTM-coordinates*
—

Dokumentkontroll/*Document control*

Kvalitetssikring i henhold til/*Quality assurance according to* NS-EN ISO9001

Rev./ *Rev.*	Revisjonsgrunnlag/*Reason for revision*	Egenkontroll/ *Self review* av/*by:*		Sidemanns-kontroll/ *Colleague review* av/*by:*		Uavhengig kontroll/ *Independent review* av/*by:*		Tverrfaglig kontroll/ *Inter-disciplinary review* av/*by:*	
0	Originaldokument	DI		PG					

Dokument godkjent for utsendelse/ *Document approved for release*	Dato/*Date*	Sign. Prosjektleder/*Project Manager*
	Oslo, 2012-05-18	for Kalle Kronholm